JOURNAL OF GEOPHYSICAL RESEARCH, VOL. 113, C01005, doi:10.1029/2006JC004031, 2008

Geometry-induced residual eddies in estuaries with curved channels: Observations and modeling studies

Chunyan Li,[1] Changsheng Chen,[2] Dominic Guadagnoli,[3] and Ioannis Y. Georgiou[4]

Received 25 November 2006; revised 26 July 2007; accepted 5 September 2007; published 9 January 2008.

[1] Observations using a vessel-based acoustic Doppler current profiler conducted in two tidal channels with significant curvatures have shown persistent residual eddies. The residual eddies are clearly related to the bend of the channel. For a channel bending toward the north, the residual eddy on the east side of the channel tends to be clockwise, and the residual eddy on the west side of the channel tends to be counterclockwise. Water in these tidal channels is mostly well mixed or weakly stratified. Motivated by these observations, an analytic model is developed to study tidally induced mean circulation in a curved channel with arbitrary depth variations. A sinusoidal channel is used to simulate the effect of curved channels. A series of experiments with different parameters have shown consistently that a pair of residual eddies around the curvature exists. By analyzing the model results, it is found that advection is a major contributor to the residual eddies. Although the pressure gradient and the nonlinear wave propagation may not be negligible, especially for long channels, it is the advection that generates the vorticity of the residual eddies. The conclusion is true for both short and long channels. Here the division between a short and long channel is 0.6 of a quarter of the tidal wavelength. In addition, we also analyzed results from a finite volume numerical model for Lake Pontchartrain, which has curved tidal channels. The results demonstrate similar residual eddies as shown by the analytical model and the observations.

Citation: Li, C., C. Chen, D. Guadagnoli, and I. Y. Georgiou (2008), Geometry-induced residual eddies in estuaries with curved channels: Observations and modeling studies, *J. Geophys. Res.*, *113*, C01005, doi:10.1029/2006JC004031.

1. Introduction

[2] Few tidal channels are straight. The curvature of tidal channels in coastal waterways and estuaries may affect the mixing [e.g., *Seim and Gregg*, 1997] and the transport of waterborne materials. For example, the nonlinear force in a curved channel can contribute to significant tidal asymmetry [*Dronkers*, 1986; *Blanton et al.*, 2002] such that flood tide and ebb tide may have different flow magnitudes thereby causing significant net (residual) circulations or the so-called tidal pumping [e.g., *Fischer et al.*, 1979]. The curvature may also generate bottom scouring and deposition which in turn modify the bottom topography and flow field and related sediment transport.

[3] The study of estuarine circulations however have largely concentrated on problems in straight channels. Although few observations are conducted in strictly straight channels, the conceptual interpretations are mostly for straight channels. For example, the early estuarine model which describes the two-layered gravitational flows (top out and bottom in) [e.g., *Hansen and Rattray*, 1965] is a straight channel. In other studies that consider the cross channel depth variations and density driven flows, straight channel models are used to demonstrate that the exchange flow develops a tendency to be channel in and shoal out [e.g., *Hamrick*, 1979; *Wong*, 1994] which may be further modified by the Coriolis force [e.g., *Valle-Levinson et al.*, 2003]. In still other models that study the effect of nonlinearity of the tidal motion, straight channel models are used to illustrate the top-in and bottom-out characteristics for well-mixed tidal channels with rectangular cross sections but without freshwater discharge [*Ianniello*, 1977, 1979]. Straight channel models are also developed allowing depth variations across the channel which show that the exchange flow pattern varies with channel length: for channels longer than 0.6 of a quarter of the tidal wavelength, the inward transport is from the shallow waters and the return flows from the deep waters; while for channels shorter than 0.6 of a quarter of the tidal wavelength, the inward transport is from the deep waters and the return flows from the shallow waters [*Li and O'Donnell*, 1997, 2005].

[4] The flow characteristics as well as associated sediment transport in curved channels have been investigated by numerous studies [e.g., *Fares*, 1995; *Ye and McCorquodale*, 1998; *Ikeda and Nishimura*, 1986]. These studies however are mostly from engineering point of views and for open

[1]Coastal Studies Institute, Department of Oceanography and Coastal Sciences, Louisiana State University, Baton Rouge, Louisiana, USA.
[2]School for Marine Science and Technology, University of Massachusetts Dartmouth, New Bedford, Massachusetts, USA.
[3]Coastal Resources Division, Department of Natural Resources, Brunswick, Georgia, USA.
[4]Department of Earth and Environmental Sciences, University of New Orleans, New Orleans, Louisiana, USA.

0148-0227/08/2006JC004031$09.00

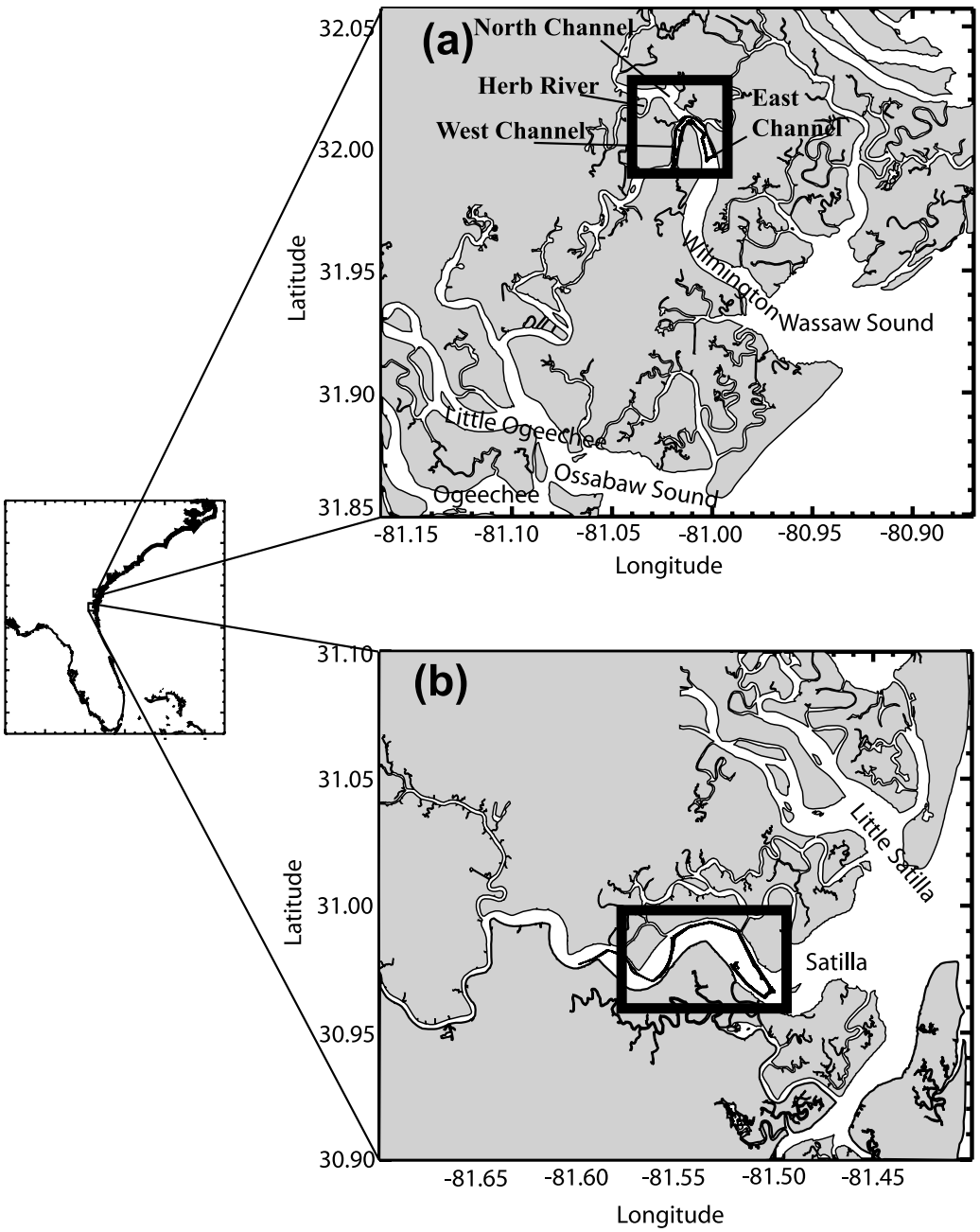

Figure 1. Study areas: (a) Wilmington River Estuary at about 32°N, 81°W, where it covers two river bends (see Figure 2 and text) and (b) Satilla River Estuary at about 30.98°N, 81.55°W, where the study covers a 90° bend. The rectangular areas show the place where field observations were conducted.

channel unidirectional flows in rivers, rather than estuaries in which tidal oscillations reverse the flow directions regularly. The existence of tidal motions complicates the dynamics significantly not only because the flow reverses directions at tidal frequencies but also because the added nonlinear process related to the finite amplitude of the surface elevation. In addition, estuaries are usually wider than alluvial rivers. An example of complicated flows under the influence of tides is that caused by headlands around which eddies form [e.g., *Pingree and Maddock*, 1977a, 1977b, 1979; *Pingree*, 1978; *Maddock and Pingree*, 1978; *Fang and Yang*, 1985; *Signell and Geyer*, 1991; *Geyer*, 1993; *Wolanski et al.*, 1996; *Chant and Wilson*, 1997]. The formation of eddies can be significant in mixing, dilution, and transport of materials. The straight channel paradigm for the theoretical studies of estuaries, where tides are significant, exists with its own right. It provides a baseline framework for conceptual understandings. The straight channel models are easier to handle mathematically and in many cases can serve as good first-order approximations.

[5] In contrast to extensive studies and conceptual models for straight channels, observations in estuaries with significant coastline variations, including the effect of channel curvature, are scarce. The study of *Seim and Gregg* [1997]

Table 1. List of Surveys in the Year 2004

Date	Moon Phase	Ship Route	Repetition	Duration, h	Tide, m
31 Aug	2 d after full moon	complex	10–15	11.75	1.32
23 Sep	2 d after first quarter moon (neap)	complex	12	12.29	1.15
29 Sep	1 d after full moon	polygon	9	11.61	1.26
17–18 Nov	first quarter moon in 2 d	hook	15	32.96	1.27

demonstrated the effect of curvature in strengthening vertical mixing over a sill. *Elston et al.* [2000] and *Elston* [2005] studied the secondary circulation in a curved channel of Satilla River Estuary. *Lacy and Monismith* [2001] studied secondary currents in a relatively straight portion of a curved channel and found that the lateral advection was important. The objectives of the present study include (1) documenting and analyzing tidal and net flow conditions around strongly curved tidal channels; (2) developing an analytic model to further study the nonlinear effect of the curvature of channel on the generation of observed net flow patterns (residual eddies); and (3) application of a numerical model to tidal channels to further verify the analytic model results. The observations presented here use a vessel-based acoustic Doppler current profiler (ADCP). By repeatedly sampling along predefined tracks several times within one or more tidal cycle(s), a distribution of the flow field can be obtained. A harmonic analysis is then applied to obtain the major tidal constituents and the net flows. The analytic model simulates the effect of the curved channel by specifying sinusoidal channel functions. Although the coastlines are straight in the model (to make it mathematically convenient to solve), the meandering channel can produce the effect of curvature. The numerical model is a finite volume coastal ocean model (FVCOM) applied to the Lake Pontchartrain system which has several meandering tidal channels.

2. Observations

[6] In order to determine the effect of channel curvature on tidal and subtidal flow structures, vessel-based observations were conducted in two different tidal channels: the Wilmington River Estuary and Satilla River Estuary (Figure 1). Both channels are located on the coast of the central South Atlantic Bight, with the former being 125 km to the northeast of the latter. Several surveys were conducted starting the year 2001. In this paper we only present results obtained during more recent surveys in which larger areas than the earlier surveys were covered. The results are quite consistent among different surveys which make it sufficient to just use the results from the larger areas. We will therefore present results from surveys conducted on 31 August and 23 and 29 September 2004 in the Wilmington River Estuary (Figure 1a) and that conducted on 17 and 18 November 2004 in the Satilla River Estuary (Figure 1b). The shortest duration of the surveys is 8.9 h on 17 November 2004. The rest of the surveys lasted between 11.6 and 12.3 h (Table 1). The 8.9 h survey is short for a harmonic analysis involving a 12 h period semidiurnal tide. Therefore we combine the data from 17 and 18 November to form a total of 33 h of time series (with a gap at the night of 17 November).

2.1. Surveys in Wilmington River Estuary

[7] As shown in Figure 1a, the study area is where the Wilmington River bifurcates. The West Channel meets the East Channel downstream of the North Channel with a bend of about 150 degrees. The North Channel is itself a bend as well near the mouth of the Herb River. The North Channel is connected to the Savannah River through a long and narrow waterway [*Li et al.*, 2006]. The influence of river discharge from the Savannah River is quite limited. The flow in the Wilmington River is thus mostly single layered.

[8] The first two surveys conducted on 31 August and 23 September 2004 have identical ship routes which consist of (1) a 2.9 km long spoon-shaped line in the North Channel, (2) a 3.4 km long polygon that covers the peripheral of the West Channel which has a 30 degree turn toward the northeast as it merges with the Wilmington River, and (3) three diagonal lines totaling about 3.1 km connecting some of the vertices of the polygon (see the insert of Figure 2a for the actual ship track). The entire route for the first two surveys is about 9.4 km in length. During the first survey on 31 August 2004, the polygon was repeated 11 times, and the spoon-shaped line in the North Channel was repeated 15 times (Table 1). The diagonal lines were repeated 10 times. During the second survey, all lines of the same route were repeated 12 times.

[9] The third survey conducted on 29 September uses a different route which is a polygon covering both the West and East Channels along the big bend (Figure 3a). The West side of this route has a similar coverage as the previous surveys though with a different route. The length of this route is about 9.5 km. The observations covered the entire route 9 times (Table 1).

2.2. Surveys in Satilla River Estuary

[10] The last two surveys were conducted between 17 and 18 November 2004, mostly during daylight time along a 90 degree bend in the middle of the Satilla River Estuary (Figure 1b). The observations covered nearly two semidiurnal tidal cycles with 15 repetitions in total (Table 1). The route is about 11 km in length and covers both the West and East sides of the bend of the channel. Note that tide in this area is essentially semidiurnal [e.g., *Pietrafesa et al.*, 1985] which makes 12-h observations sufficient to resolve the main tidal constituents.

2.3. Observational Setup

[11] During all the surveys, an 8 m long twin-engine research vessel was used to repeatedly occupy a predefined route to measure current velocity profiles using a RDI 600 kHz acoustic Doppler current profiler (ADCP). The ADCP was mounted on one side of the boat approximately 0.4 m below the surface. A 0.5 m vertical bin was used to record the data. The surveys were conducted at an

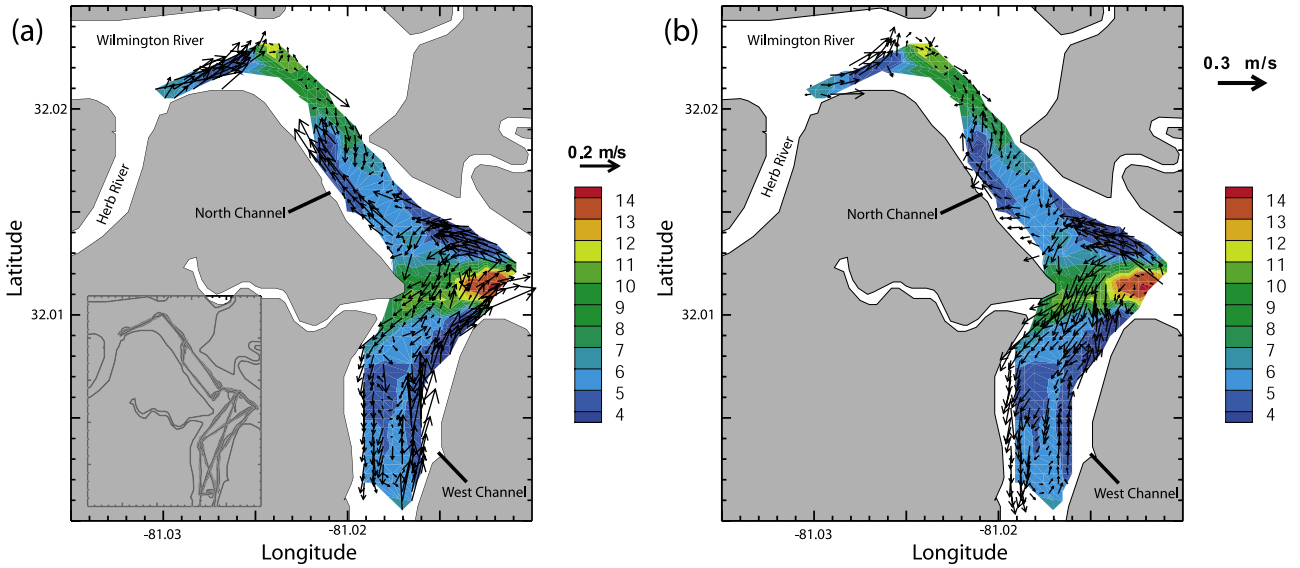

Figure 2. Residual transport velocity calculated from the observations in Wilmington River Estuary: results from (a) the survey conducted on 31 August 2004 and (b) the survey conducted on 23 September 2004. Note that the residual transport velocity is the total vertically averaged mean velocity, an Eulerian, not a Lagrangian, quantity. The colored contours show the mean depth obtained from ADCP.

average cruise speed of about 2.5–3 m/s except at the turns when the vessel had to slow down and during CTD casts when the vessel had to stop for a few minutes. A Seabird Electronic SBE 19 plus CTD was used to measure the vertical profiles of water temperature, salinity, fluorescence, light attenuation, and dissolved oxygen at two to three locations during each survey.

2.4. Results

[12] In general, the horizontal flow is unidirectional in the vertical water column at all times in these surveys. The vertical profiles of the temperature and salinity during the 29 September survey show (Figure 4 for salinity) that the water column was close to well mixed conditions within most of the tidal cycle except during the low tide when stratification existed (with 2 PSU change of salinity over 5 m) which may be attributed to the effect of tidal straining [*Simpson et al.*, 1990]. Because of the vertically well mixed nature, the tidal flow is mostly barotropic except during low tide for a short period (within 1 hour or shorter). After applying a harmonic analysis [*Li et al.*, 2000, 2004; *Li*, 2002], the depth averaged residual flow field is obtained for each survey.

[13] The magnitude of the depth-averaged velocity components is ~0.6–0.9 m/s and the subtidal depth-averaged velocity is significantly smaller which is mostly within 0.05–0.20 m/s. The velocity amplitude for the east and north components appear to be inversely related; that is, larger east velocity corresponds to smaller north velocity and vice versa. This is simply because the majority of the flow tends to be along the channel and the cross channel velocity component is relatively smaller. For example, when the channel orientation is north and south, the velocity is mainly north-south directed and thus the north component is much larger than the east component. This is similar to the findings in a tidal creek [*Li et al.*, 2004]. The depth

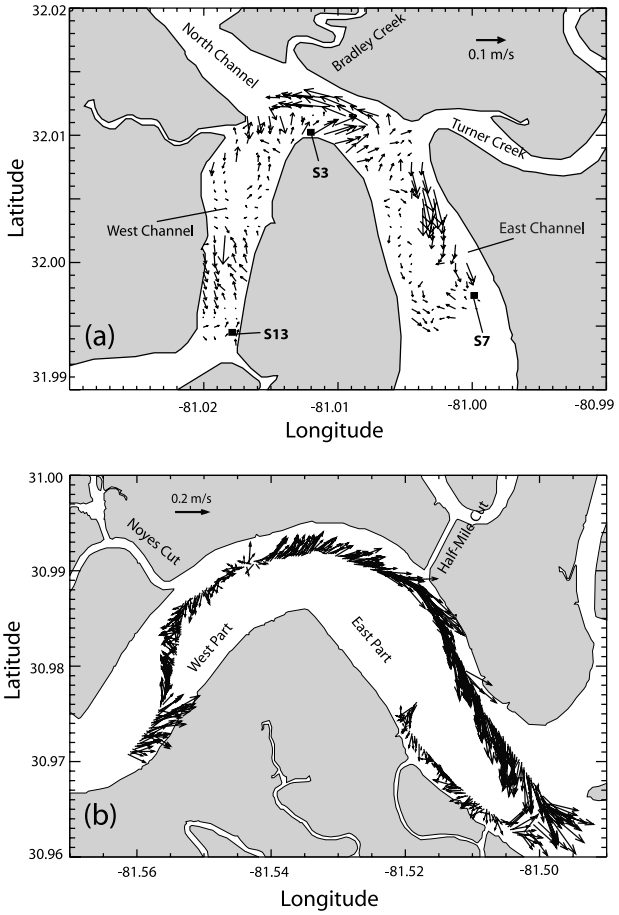

Figure 3. Residual transport velocity calculated from the observations in (a) Wilmington River Estuary conducted on 29 September 2004 and (b) Satilla River Estuary conducted on 17–18 November 2004.

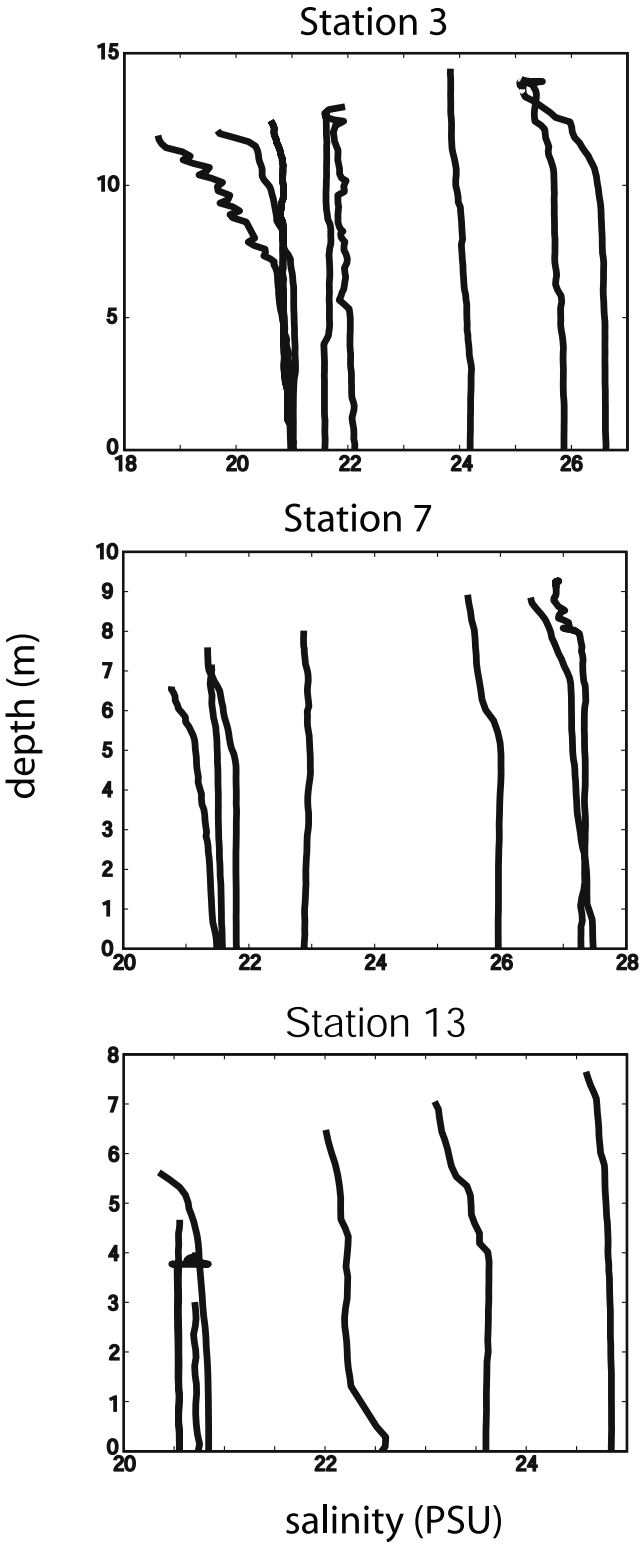

Figure 4. Vertical profiles of salinity from observations conducted on 29 September 2004 from three stations as indicated in Figure 3a, i.e., the points marked by S3, S7, and S13, which are located at 32°0.666, 81°0.748; 31°59.854, 80°59.957; and 31°59.638, 81°1.081, respectively.

averaged velocity amplitude is slightly smaller than the near surface counterparts, apparently a result of bottom friction.

[14] Figure 2a shows the residual flow field for the 31 August survey. The maximum residual velocity is 0.32 m/s with an average of about 0.11 m/s and a standard deviation of 0.07 m/s (Table 2). The vectors of the residual flow field show some interesting eddies or reversing currents across the channels. More specifically, the east side of the West Channel is dominated by the strong northward and northeastward residual flows; while the west side of the West Channel is dominated by weaker southward and southwestward flows. Between these two opposing flows the currents in the middle of the channel is much weaker. This pattern of reversing flows is merged with the eddy-like flow pattern at the intersection of the three channel (the West, East, and North Channels) where it shows a counterclockwise eddy. Further to the northwest into the north channel opposing flows also appear across the channel such that the westside of the channel has a relatively strong northwestward flow contrasted by a weaker southward flow on the other side of the channel. At the northwest corner of the survey area, the residual flow is quite strong toward the northeast, appearing to be part of another recirculation pattern.

[15] The 23 September survey covered the same area using the same survey route as that of 31 August (Figure 2b). The maximum residual velocity is 0.28 m/s with an average of about 0.10 m/s and a standard deviation of 0.06 m/s (Table 2). The vectors of the residual flow field again show some eddies and reversing currents across the channels, similar to the earlier results. The 31 August survey was conducted 2 d after the full moon while the 23 September survey was conducted during a neap tide (Table 1). The first survey had a slightly larger maximum residual flow (0.32 versus 0.28 m/s), but roughly the same mean residual flow (0.11 versus 0.10 m/s) and comparable standard deviations (0.07 versus 0.06 m/s).

[16] The residual flows for the 29 September survey are shown in Figure 3a. This survey covered the West and East Channels but not the North Channel. The maximum residual velocity is 0.19 m/s with an average of only about 0.05 m/s and a standard deviation of 0.04 m/s (Table 2). The vectors of the residual flow field also show some reversing currents across the channels.

[17] Figure 3b shows the residual flow field for the 17–18 November surveys. The maximum residual velocity is 0.34 m/s with an average of about 0.08 m/s and a standard deviation of 0.09 m/s (Table 2). The south side of the western part of the channel is dominated by northeastward residual flows (downstream from the river to the ocean); while the north side of it is dominated by westward or southward flows. Between these two opposing flows, the currents in the middle of the channel appear to be in transition. This flow pattern suggests a similar eddy-like

Table 2. Statistics of Residual Flows

Date	Average, m/s	Maximum, m/s	Standard Deviation
31 Aug	0.106	0.310	0.071
23 Sep	0.098	0.283	0.059
29 Sep	0.046	0.189	0.040
17–18 Nov	0.084	0.338	0.091

opposing structure as seen in the earlier surveys conducted in the Wilmington River as discussed above. Along the outside of the eastern part of the channel, the flow is basically downstream curving with the channel and coastline. The south side of the eastern part of the channel shows a weak and variable flow pattern. The bathymetry of the Wilmington study area is shown by the colored contour plots of Figure 2. The bathymetry of the Satilla River study area is such that the deep channel is about 8 to 11 m and the ship track is mostly in the channel.

2.5. Summary of Observational Findings

[18] Although there are quite a lot of variabilities among these survey results, a common feature appear to be persistent. This common feature is that the flows on the eastern side of the channel, which bends toward the north, tend to have clockwise residual eddies and the flows on the western side of the bend tend to have counterclockwise residual eddies. This tendency of course is subject to modification by the complex geometry and changing forcing conditions. These forcing conditions may include local wind effects, river discharge, remote wind effects, etc. These factors are likely of secondary importance unless under extreme weather conditions. Since the surveys were all conducted under favorable weather, the patterns of the residual flow field are quite consistent. The consistent flow features motivate the authors to a further investigation using an analytic model. The basic hypothesis is that the residual eddies are generated by nonlinear tidal rectification under the influence of bathymetry and river bend. Effects of wind and river discharge are thus neglected here.

3. Analytic Model

[19] The model starts with the nonlinear two-dimensional equations, i.e.,

$$\begin{aligned} &\frac{\partial \mathbf{v}}{\partial t} + (\mathbf{v}\cdot\nabla)\mathbf{v} = -g\nabla\zeta - \beta\frac{\mathbf{v}}{h} + \frac{\beta}{h^2}\mathbf{v}\zeta \\ &\frac{\partial \zeta}{\partial t} + \nabla\cdot[(h+\zeta)\mathbf{v}] = 0, \quad \mathbf{v} = (u,v) \end{aligned} \tag{1}$$

in which u, v, ζ, x, y, t, β, g, h are the along channel and cross channel velocities, surface elevation, along and cross channel coordinates, time, frictional coefficient, gravitational acceleration, and local mean water depth, respectively. The frictional coefficient β is expressed as $\beta = \frac{8C_D U_0}{3\pi}$ where C_D and U_0 are the bottom drag coefficient and the magnitude of the longitudinal velocity, respectively. The local mean water depth is time-averaged depth at a given location and is thus a function of x and y. In (1) the quadratic friction has been decomposed into a linear part and a higher-order term correct to the second order as shown by, e.g., *Proudman* [1953] and *Parker* [1984] and used by *Li and O'Donnell* [1997, 2005].

[20] The depth as a function of x and y is written as

$$h = h_0(1 + \gamma h_1) \tag{2}$$

where h_0 and γ are constants, and h_1 is a specified dimensionless function of x and y. In order to solve the problem analytically, we assume that γ is a number smaller than $\mathcal{O}(1)$. The depth range is thus $\delta h = \gamma h_0 \delta h_1$. We further require that the range of h_1 or δh_1 is of $\mathcal{O}(1)$. Therefore γ is a nondimensional measure of the variation of the depth function and is roughly proportional to $(h_{\max} - h_{\min})/h_0$.

[21] By using a scaling analysis and the following relations, the above equations are nondimensionalized

$$\begin{aligned} &\hat{t} = \sigma t, \;\; \hat{x} = \frac{x}{L}, \;\; \hat{y} = \frac{y}{D}, \;\; \hat{u} = \frac{u}{U}, \;\; \hat{v} = \frac{v}{V}, \;\; \hat{h} = \frac{h}{h_0}, \\ &\tilde{\zeta} = \frac{\zeta}{a}, \;\; U = a\sqrt{\frac{g}{h_0}} \\ &V = \epsilon\sigma D, \;\; \epsilon = \frac{a}{h_0}, \;\; L = \frac{\lambda}{2\pi} = \frac{T\sqrt{gh_0}}{2\pi}, \;\; T = \frac{2\pi}{\sigma} \end{aligned} \tag{3}$$

to yield

$$\begin{aligned} &\frac{\partial u}{\partial t} + \epsilon u\frac{\partial u}{\partial x} + \epsilon v\frac{\partial u}{\partial y} = -\frac{\partial \zeta}{\partial x} - \mathcal{D}\frac{u}{h} + \epsilon\mathcal{D}\frac{u\zeta}{h^2} \\ &\frac{\partial v}{\partial t} + \epsilon u\frac{\partial v}{\partial x} + \epsilon v\frac{\partial v}{\partial y} = -\mathcal{H}\frac{\partial \zeta}{\partial y} - \mathcal{D}\frac{v}{h} + \epsilon\mathcal{D}\frac{v\zeta}{h^2} \\ &\frac{\partial \zeta}{\partial t} + \frac{\partial (h+\epsilon\zeta)u}{x} + \frac{\partial (h+\epsilon\zeta)v}{y} = 0 \end{aligned} \tag{4}$$

where σ, L, D, U, V, a, and T are the angular frequency of semidiurnal tide, the tidal length scale, the width of the channel, the magnitude of the longitudinal velocity, the magnitude of the lateral velocity, the tidal amplitude at the mouth, and the period of the tide, respectively. The variables u, v, ζ etc. are nondimensional (i.e., $\hat{u}$, $\hat{u}$, $\hat{\zeta}$, etc.) as defined in (3). The carets have been omitted for clarity. The parameter $\mathcal{D}$ is $\frac{\beta}{\sigma h_0}$ and the coefficient of the cross channel pressure gradient $\mathcal{H}$ is $\left(\frac{\sqrt{gh_0}}{\sigma D}\right)^2$. Omitting the caret, the dimensionless depth is

$$h = 1 + \gamma h_1 \tag{5}$$

[22] The basic idea of the solution is to make a perturbation expansion for the above equations in terms of the nonlinear parameter ϵ:

$$\epsilon = \frac{\zeta_0}{h_0} < 1 \tag{6}$$

and solve the first-order (linear) and second-order solutions separately; that is, we assume a power series expansion for the velocity and elevation in terms of ϵ

$$\mathbf{v} = \mathbf{v}_0 + \epsilon\mathbf{v}_1 + \epsilon^2\mathbf{v}_2 + \cdots, \;\; \zeta = \zeta_0 + \epsilon\zeta_1 + \epsilon^2\zeta_2 + \cdots \tag{7}$$

in which

$$\mathbf{v}_i = \mathbf{v}_i(x,y,t), \quad (i = 0,1,2,\cdots), \;\; \zeta_i = \zeta_i(x,y,t) \tag{8}$$

[23] By substituting (7) into (4), the $\mathcal{O}(\epsilon^0)$ equations, and the $\mathcal{O}(\epsilon^1)$ equations are obtained, respectively, as

$$\begin{aligned}\frac{\partial u_0}{\partial t} &= -\frac{\partial \zeta_0}{\partial x} - \mathcal{D}\frac{u_0}{h}\\ \frac{\partial v_0}{\partial t} &= -\mathcal{H}\frac{\partial \zeta_0}{\partial y} - \mathcal{D}\frac{v_0}{h}\\ \frac{\partial \zeta_0}{\partial t} &+ \frac{\partial h u_0}{\partial x} + \frac{\partial h v_0}{\partial y} = 0\end{aligned} \tag{9}$$

$$\begin{aligned}\frac{\partial u_1}{\partial t} + u_0\frac{\partial u_0}{\partial x} + v_0\frac{\partial u_0}{\partial y} &= -\frac{\partial \zeta_1}{\partial x} - \mathcal{D}\frac{u_1}{h} + \mathcal{D}\frac{u_0\zeta_0}{h^2}\\ \frac{\partial v_1}{\partial t} + u_0\frac{\partial v_0}{\partial x} + v_0\frac{\partial v_0}{\partial y} &= -\mathcal{H}\frac{\partial \zeta_1}{\partial y} - \mathcal{D}\frac{v_1}{h} + \mathcal{D}\frac{v_0\zeta_0}{h^2}\\ \frac{\partial \zeta_1}{\partial t} + \frac{\partial h u_1}{\partial x} + \frac{\partial \zeta_0 u_0}{\partial x} &+ \frac{\partial h v_1}{\partial y} + \frac{\partial \zeta_0 v_0}{\partial y} = 0\end{aligned} \tag{10}$$

The $\mathcal{O}(\epsilon^0)$ problem is forced by sea level at the open end of the channel ($x = 0$) which is specified as

$$\zeta_0|_{x=0} = e^{jt} \tag{11}$$

and the no-normal flow at the closed end and sides is enforced by the boundary conditions

$$u_0|_{x=1} = 0, \quad v_0|_{y=0,1} = 0 \tag{12}$$

[24] We assume that the channel has parallel lateral boundaries. The curvature of the deep channel will be expressed by the depth function, rather than the coastline, as demonstrated below. Equation (9) is linear with variable coefficients in the friction and continuity divergence terms. To solve the $\mathcal{O}(\epsilon^0)$ problem, (9), the functions are expanded in terms of the bottom slope parameter γ (>0) with the condition that γ is smaller than 1. The expansions are then

$$\begin{aligned}&u_0 = u_{00} + \gamma u_{01} + \gamma^2 u_{02} + \cdots, \quad v_0 = v_{00} + \gamma v_{01} + \gamma^2 v_{02} + \cdots\\ &\zeta_0 = \zeta_{00} + \gamma\zeta_{01} + \gamma^2\zeta_{02} + \cdots\end{aligned} \tag{13}$$

Note that only the $\mathcal{O}(\epsilon^0)$ variables are expanded in γ, and that the $\mathcal{O}(\epsilon^0)$ and $\mathcal{O}(\epsilon^0\gamma^0)$ are different. The former includes the effect of the bathymetry and the latter does not; the latter is only the first term expanded in terms of γ from $\mathcal{O}(\epsilon^0)$. The expansion in γ is used to obtain an approximate solution to the $\mathcal{O}(\epsilon^0)$ problem and this is used to force the $\mathcal{O}(\epsilon^1)$ problem which is the lowest order at which a residual circulation can be resolved.

[25] For a depth function given by (5), since

$$\frac{1}{h} = \frac{1}{1+\gamma h_1} = \sum_{i=0}^{\infty}(-1)^i(\gamma h_1)^i = 1 - \gamma h_1 + \gamma^2 h_1^2 + \cdots \tag{14}$$

the problem can be restated as a series of equations $\mathcal{O}(\epsilon^0\gamma^i)$:

$$\begin{aligned}&\frac{\partial u_{0i}}{\partial t} = -\frac{\partial \zeta_{0i}}{\partial x} - \mathcal{D}u_{0i} + \tilde{F}_{xi}, \quad \frac{\partial v_{0i}}{\partial t} = -\frac{\partial \zeta_{0i}}{\partial y} - \mathcal{D}v_{0i} + \tilde{F}_{yi}\\ &\frac{\partial \zeta_{0i}}{\partial t} + \frac{\partial u_{0i}}{\partial x} + \frac{\partial v_{0i}}{\partial y} = \tilde{F}_{zi}\end{aligned} \tag{15}$$

where i = 0, 1, .., M; and the error resulting from the truncation of the expansion is $\mathcal{O}(\epsilon^0\gamma^{M+1})$, and

$$\begin{aligned}(\tilde{F}_{xi}, \tilde{F}_{yi}) = &-\mathcal{D}[-(u_{0,i-1}, v_{0,i-1})h_1 + (u_{0,i-2}, v_{0,i-2})h_1^2 + \cdots\\ &+ (-1)^m(u_{0,i-m}, v_{0,i-m})h_1^m + \cdots\\ &+ (-1)^i(u_{0,0}, v_{0,0})h_1^i]\\ \tilde{F}_{zi} = &-\frac{\partial h_1 u_{0,i-1}}{\partial x} - \frac{\partial h_1 v_{0,i-1}}{\partial y}\end{aligned} \tag{16}$$

The largest neglected term in the $\mathcal{O}(\epsilon^0\gamma^M)$ solution is $\mathcal{O}(\epsilon^0\gamma^{M+1})$. Since the error for u_0, v_0, ζ_0 is $\mathcal{O}(\epsilon^1)$, consistency requires that $\gamma^{M+1} \sim \epsilon^1$ which yields $M = \left[\frac{2\log_e \varepsilon}{\log_e \gamma} - 1\right] + 1$ where the brackets, [ ], indicate the largest integer not bigger than the number inside. For instance, for $\epsilon = 0.1$, $\gamma = 0.5$, $M = [2.3] + 1 = 3$. Therefore three terms for u_0 are enough in this example.

[26] Since all the systems of the $\mathcal{O}(\epsilon^0\gamma^i)$ equations above are linear and the tidal forcing frequency is σ, the solution for u_{0i}, v_{0i} and ζ_{0i} can be expressed as

$$(u_{0i}, u_{0i}) = Re\{(U_i, V_i)e^{jt}\}, \quad \zeta_{0i} = Re\{A_i e^{jt}\} \tag{17}$$

where $Re\{\}$ indicates the real part of the complex function inside the braces. Denoting

$$(\tilde{F}_{xi}, \tilde{F}_{yi}) = Re\{(F_{xi}, F_{yi})e^{jt}\}, \ \tilde{F}_{zi} = Re\{F_{zi}e^{jt}\} \tag{18}$$

then

$$\begin{aligned}(F_{xi}, F_{yi}) = &-\mathcal{D}[-(U_{i-1}, V_{i-1})h_1 + (U_{i-2}, V_{i-2})h_1^2 + \cdots\\ &+ (-1)^m(U_{i-m}, V_{i-m})h_1^m + \cdots + (-1)^i(U_0, V_0)h_1^i]\\ F_{zi} = &-\left(\frac{\partial h_1 U_{i-1}}{\partial x} + \frac{\partial h_1 V_{i-1}}{\partial y}\right)\end{aligned} \tag{19}$$

[27] Substituting (17) into (15) and with some straightforward algebra, equations for A_i, U_i, and V_i can be obtained [*Li*, 2006], the solution of which is provided in the appendix of *Li* [2006].

[28] It is obvious that the $\mathcal{O}(\epsilon^0\gamma^0)$ solution, (u_{00}, v_{00}, ζ_{00}), is the first-order approximation and therefore A_0, U_0 and V_0 are already solved. *Li and O'Donnell* [1997] used this first-order solution to solve the second-order residual circulation, which means that only the $\mathcal{O}(\epsilon^0\gamma^0)$ term is used to approximate $\mathcal{O}(\epsilon^0)$. After A_k, U_k and V_k (k = 0, 1, 2, $\cdots$, $i-1$) are solved, A_i, U_i and V_i can then be derived. Thus ζ_0, u_0 and v_0 can be found using (13) and (17). The solution for A_i (i = 1, 2,) using Fourier Series is given by *Li* [2006].

[29] Now that the $\mathcal{O}(\epsilon^0)$ equations have been solved for u_0, v_0 and ζ_0 with an error of $\mathcal{O}(\epsilon^1\gamma^{M+1})$, assuming that $M+1$ terms are used for each variable for the approximation, the solution of the $\mathcal{O}(\epsilon^1)$ problem can be addressed. Since we are dominantly interested in the mean circulation, equations (10) are averaged to obtain

$$\begin{aligned}\overline{u_0\frac{\partial u_0}{\partial x}} + \overline{v_0\frac{\partial u_0}{\partial y}} &= -\frac{\partial \overline{\zeta}_1}{\partial x} - \mathcal{D}\frac{\overline{u}_1}{h} + \mathcal{D}\overline{\frac{u_0\zeta_0}{h^2}}\\ \overline{u_0\frac{\partial v_0}{\partial x}} + \overline{v_0\frac{\partial v_0}{\partial y}} &= -\mathcal{H}\frac{\partial \overline{\zeta}_1}{\partial y} - \mathcal{D}\frac{\overline{v}_1}{h} + \mathcal{D}\overline{\frac{v_0\zeta_0}{h^2}}\\ \frac{\partial h\overline{u}_1}{\partial x} + \frac{\partial \overline{\zeta_0 u_0}}{\partial x} &+ \frac{\partial h\overline{v}_1}{\partial y} + \frac{\partial \overline{\zeta_0 v_0}}{\partial y} = 0\end{aligned} \tag{20}$$

with $\mathcal{O}(\epsilon^2)$ error, and the boundary conditions are

$$\overline{u}_1|_{x=1} = 0, \quad \overline{v}_1|_{y=0,1} = 0 \tag{21}$$

[30] The dimensional total (vertically integrated) residual transport (an Eulerian quantity), obtained by integrating the velocity vertically from the bottom to the surface, expressed in components, is

$$T_u = \overline{u^d\left(\zeta^d + h^d\right)}, \quad T_v = \overline{v^d\left(\zeta^d + h^d\right)} \tag{22}$$

where the superscript "d" indicates a dimensional quantity to avoid confusion. Dividing the above equations by the mean depth h^d, we obtain a quantity with a unit of velocity:

$$u_T^d = \frac{T_u}{h^d} = \overline{u^d\left(\zeta^d + h^d\right)},; \quad v_T^d = \frac{T_v}{h^d} = \overline{v^d\left(\zeta^d + h^d\right)} \tag{23}$$

In other words, when the quantity (u_T^d, v_T^d) is multiplied by the mean depth, it is the total transport in the entire water column of unit width, i.e., $(\overline{u^d\left(\zeta^d + h^d\right)}, \overline{v^d\left(\zeta^d + h^d\right)})$. Note that this velocity is an Eulerian quantity. The dimensionless form of this velocity can be expressed as

$$\overline{u}_T = \frac{\overline{u}_T^d}{U} = \overline{u} + \epsilon\frac{\overline{\zeta u}}{h}, \quad \overline{v}_T = \frac{\overline{v}_T^d}{V} = \overline{v} + \epsilon\frac{\overline{\zeta v}}{h} \tag{24}$$

[31] Since the tidally averaged $\mathcal{O}(\epsilon^0)$ solution is zero for a weakly nonlinear problem, i.e., $\overline{u}_0 = 0$ and $\overline{v}_0 = 0$, the above equation reduces to

$$\overline{u}_T = \epsilon\left(\overline{u}_1 + \frac{\overline{\zeta_0 u_0}}{h}\right) + \mathcal{O}(\epsilon^2), \quad \overline{v}_T = \epsilon\left(\overline{v}_1 + \frac{\overline{\zeta_0 v_0}}{h}\right) + \mathcal{O}(\epsilon^2) \tag{25}$$

[32] From the momentum equation, (20), the residual transport velocity components are

$$\begin{aligned}
\overline{u}_T &= \epsilon\left[2\frac{\overline{u_0\zeta_0}}{h} - \frac{h}{\mathcal{D}}\left(\overline{u_0\frac{\partial u_0}{\partial x}} + \overline{v_0\frac{\partial u_0}{\partial y}}\right) - \frac{h}{\mathcal{D}}\frac{\partial\overline{\zeta_1}}{\partial x}\right] + \mathcal{O}(\epsilon^2) \\
&= \overline{u}_{T1} + \overline{u}_{T2} + \overline{u}_{T3} \\
\overline{v}_T &= \epsilon\left[2\frac{\overline{v_0\zeta_0}}{h} - \frac{h}{\mathcal{D}}\left(\overline{u_0\frac{\partial v_0}{\partial x}} + \overline{v_0\frac{\partial v_0}{\partial y}}\right) - \frac{\mathcal{H}h}{\mathcal{D}}\frac{\partial\overline{\zeta_1}}{\partial y}\right] + \mathcal{O}(\epsilon^2) \\
&= \overline{v}_{T1} + \overline{v}_{T2} + \overline{v}_{T3}
\end{aligned} \tag{26}$$

in which $\overline{u}_{T1}$, $\overline{u}_{T2}$, and $\overline{u}_{T3}$ are the three components for the longitudinal residual velocity identified by *Li and O'Donnell* [1997, 2005] and *Li* [2006]

$$\begin{aligned}
&\overline{u}_{T1} = 2\frac{\overline{\zeta_0 u_0}}{h}\epsilon^1, \ \overline{u}_{T2} = -\frac{h}{\mathcal{D}}\left(\overline{u_0\frac{\partial u_0}{\partial x}} + \overline{v_0\frac{\partial u_0}{\partial y}}\right)\epsilon^1, \\
&\overline{u}_{T3} = -\frac{h}{\mathcal{D}}\frac{\partial\overline{\zeta}_1}{\partial x}\epsilon^1
\end{aligned} \tag{27}$$

The equation for the three components of the lateral residual velocity is similar.

4. Analytic Model Results and Discussion

[33] By applying the above model solution to bathymetry functions with meandering channels, we examine the effect of channel curvature on the residual circulation. As shown in Figure 5 these bathymetry functions are defined in channels with parallel coastlines but with an identifiable meandering deep channel. The parallel coastline makes the problem much more simplified such that we can use the above solution of a rectangular basin. The meandering deep channel allows us to simulate the effect of curvature although water exchange between the curved deep channel and the shallow shoals is possible. Note also that the minimum depth over the shoal cannot be too small to ensure the convergence of the model. In theory, the ratio between the depth variation and the mean depth should be smaller than 1.

[34] Eighteen such bathymetry functions are used in the calculations to examine the effect of channel meandering on the tidally induced residual flows. For brevity, here we only show results from four of these eighteen calculations. The domain is 3 km × 25 km, or 3 km × 55 km, representing a short channel and a long channel. The water depth ranges between 5 and 8 m (Figure 5). The domain is open at $x = 0$, where tidal forcing is introduced. The domain is closed at $x = L$ (either 25 or 55 km). Two bathymetry functions differ at the open end: the 8 m deep channel is either located close to the lateral edge of the domain or in the middle. In the limit of $h \approx 0$ on the shoal, the model domain would be reduced to a pure meandering channel with no shoals, only a channel with a slope. In that case, the analytic model is no longer valid. In general, if the depth over the shoal is small enough such that $(h_{\max} - h_{\min})/h_0 > 1$, the model would not provide convergent results. It is a unique characteristic that the model has to be rectangular and it is both a useful character and a drawback of the method. By allowing nonzero depth outside of the main channel, we allow water exchange between the channel and the shoal and at the same time we keep the problem mathematically simple and analytically tractable. As a result, there is no need to deal with a complicated boundary condition which would have been required if the lateral boundary is not straight. The drawback is that the depth of the shoal is limited to relatively large values. In all the calculations, the model does provide robust results when it is convergent.

[35] In the calculations, we choose the bottom drag coefficient to be 0.0025. A semidiurnal tide is introduced at the open end with a uniform amplitude of 1 m across the channel. Ten terms are chosen for the perturbation expansion with respect to the depth ratio parameter and ten terms are used for the Fourier series [*Li*, 2006, appendix] in calculating each of the perturbation expansion for the tidal solution.

[36] All the eighteen model runs give similar results of residual eddies. The most distinctive feature is the persistence of residual eddies on the two sides of a channel bend. For an observer (indicated by the letter "O" in Figure 6) standing in the shallow water facing the deep water in the positive y direction (with $x = 0$ on the left hand side), the

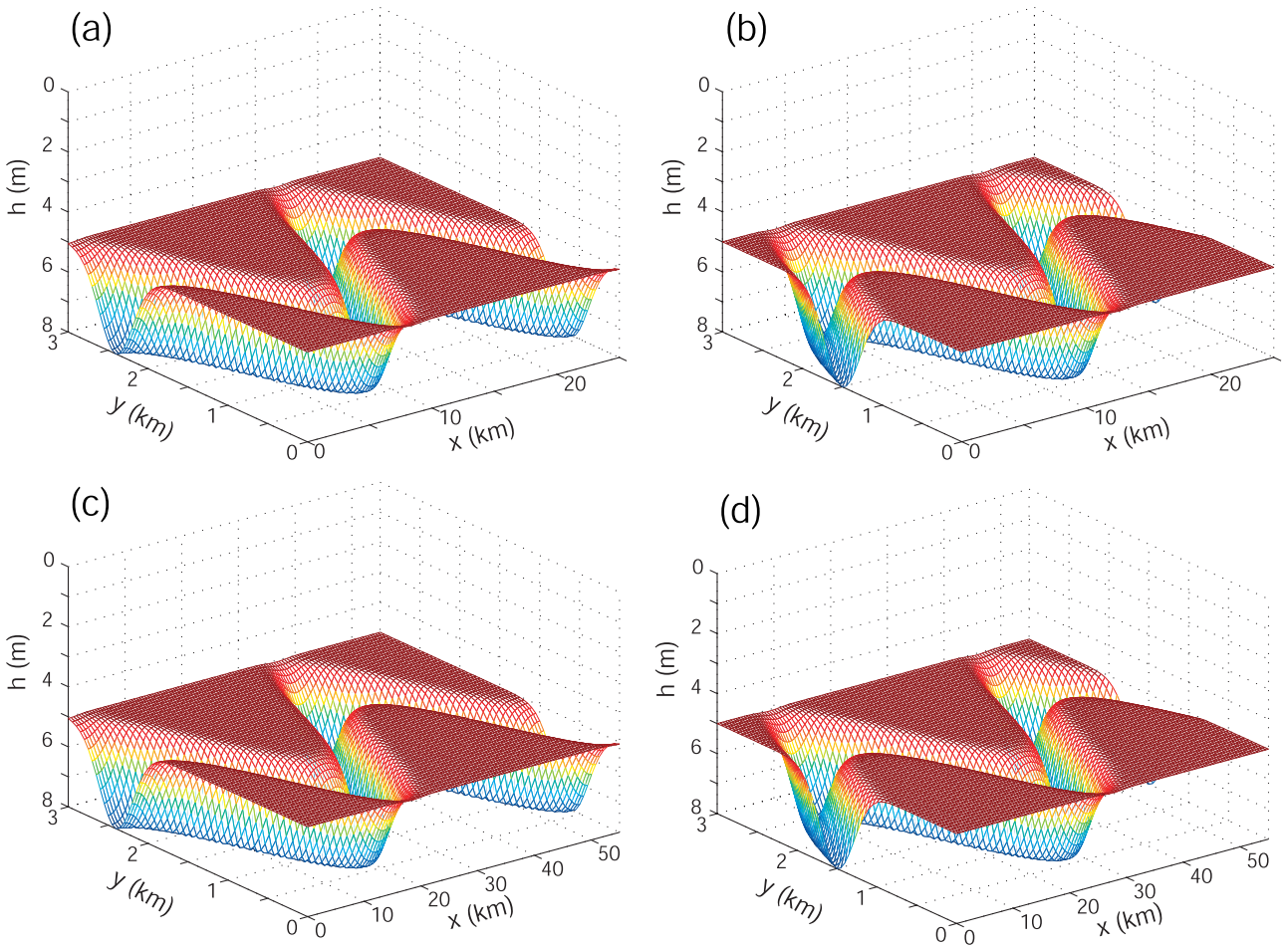

Figure 5. Bathymetry functions used in the calculations: (a and b) short channels (L = 25 km) with different positions of the channel and (c and d) long channels (L = 55 km) at the mouth.

residual flow within the deep channel on the left hand side of the observer is counterclockwise while on the right hand side it is clockwise. Outside of the deep channel, the residual flow becomes significantly smaller in general. The magnitude of the residual flow also diminishes away from the open end. These features are similar between the relatively short and long channels. The residual eddies are qualitatively the same as those observed in the field measurements discussed earlier. In addition, there is a persistent weak cross channel flow from the shoal to the deep water along the y direction at the channel bends as indicated by the arrows in Figure 6. There has been no attempt however to measure this weak cross channel flow in situations where salt marshes exist around a meandering channel. The pair of residual eddies are similar to those observed around headlands [*Geyer*, 1993]. The headland eddies however do not necessarily cross the entire channel; that is, they may be eddies limited to the vicinity of the headland feature. In contrast, the residual eddies in a curved channel are usually elongated occupying the entire channel. This may have significant implications to the cross channel and along channel mixing over timescales longer than a tidal cycle.

[37] As shown by *Li and O'Donnell* [1997, 2005], the residual circulation can be decomposed into three different contributions: the nonlinear wave plus the nonlinear bottom friction (u_{T1}), the advection (u_{T2}), and the second-order pressure gradient (u_{T3}). To examine these three contributions to the flow field in meandering channels, we calculate them for the along channel flows and the correspondent percentage of contributions as defined by [*Li*, 2006]

$$C_i = \frac{|u_{Ti}|}{\sum_{j=1}^{3} |u_{Tj}|} \tag{28}$$

[38] A similar relation can be written for the cross channel velocity component. Figure 7 shows the three components of the residual velocity in the along channel direction with the second bathymetry function for a short channel (L = 25 km) as defined in Figure 5b. The nonlinear wave and nonlinear bottom friction (u_{T1}) make only a small contribution (~0.03 m/s) although in the channel near the open end ($x \sim 0$) the magnitude of u_{T1} is relatively larger (Figure 7 (top)). It is obvious that the effect of the meandering channel shapes the different contributions along the channel in a meandering manner (Figure 7). The advection makes a relatively large contribution (~0.2 m/s) along the deep

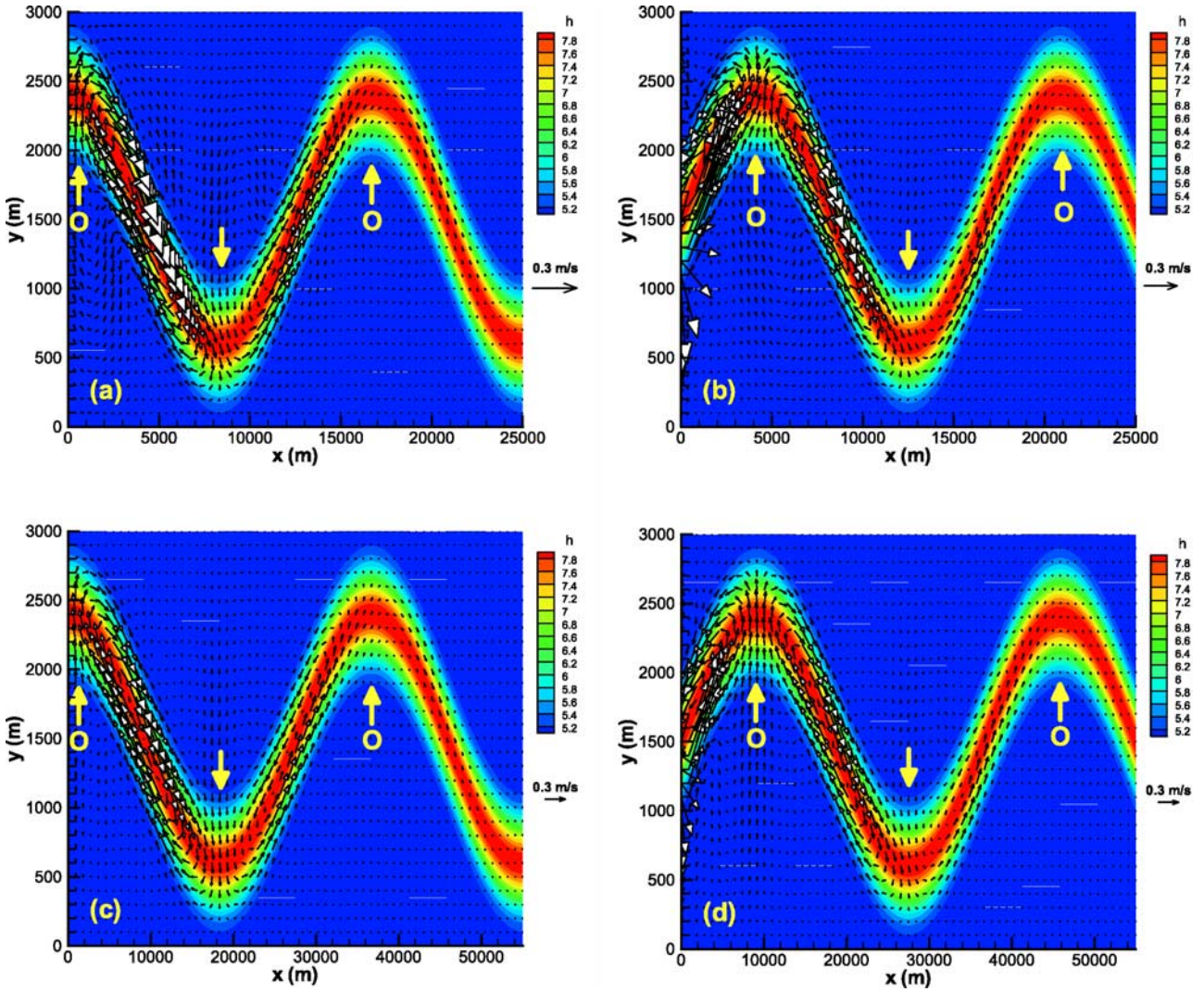

Figure 6. Residual circulations obtained using the bathymetry functions of Figure s 5a–5d.

channel (Figure 7 (middle)). It is interesting that the positive and negative advective contribution u_{T2} alternates across the channel and channel bends. This alternation does not occur in either u_{T1} or u_{T3}, indicating that the residual eddies are specifically generated by the advective nonlinearity, not the other two mechanisms. Indeed, the pressure gradient contribution u_{T3} is relatively small (~0.07 m/s).

[39] Figure 8 shows the three components of the residual velocity in the along channel direction with the third bathymetry function for a long channel (L = 55 km) as defined in Figure 5c. The nonlinear wave and nonlinear bottom friction (u_{T1}) now make a larger contribution especially at the open end where the magnitude can reach ~0.16 m/s (Figure 8 (top)). The advection still makes a relatively large contribution (~0.28 m/s) along the deep channel (Figure 8 (middle)). It is also obvious that the positive and negative advective contribution u_{T2} alternates across the channel and channel bends. The pressure gradient contribution u_{T3} is now larger (~0.26 m/s) compared to the short channel results. Despite the larger values of u_{T1} and u_{T3}, the advective contribution (u_{T2}) is still the only component that causes the alternating flow field that generates the residual eddies. The other two mechanisms can only cause unidirectional flows. In straight channels, *Li and O'Donnell* [2005] show that the residual flow reverses directions between long and short channels. Here the division between long and short channels is 0.6 of a quarter of the tidal wavelength. The results obtained here for curved long channels show that the wave induced effect and the pressure gradient effect are indeed much larger compared to their short channel counterparts. However, the effect of the curvature is so large that the advective nonlinearity is always dominant in the cases studied such that results between short and long channels do not differ significantly from that in straight channels. These results are representative of all cases studied.

[40] In the calculation, the x and y directions have 63 and 41 points, respectively. This yields a total of 2583 points of calculation on the two dimensional model domain. Using equation (28), and using results from a short channel, the maximum contributions to the total net flow at an individual point from the first, second, and third terms, are calculated to be 40.9%, 70%, and 98%, respectively. The spatial

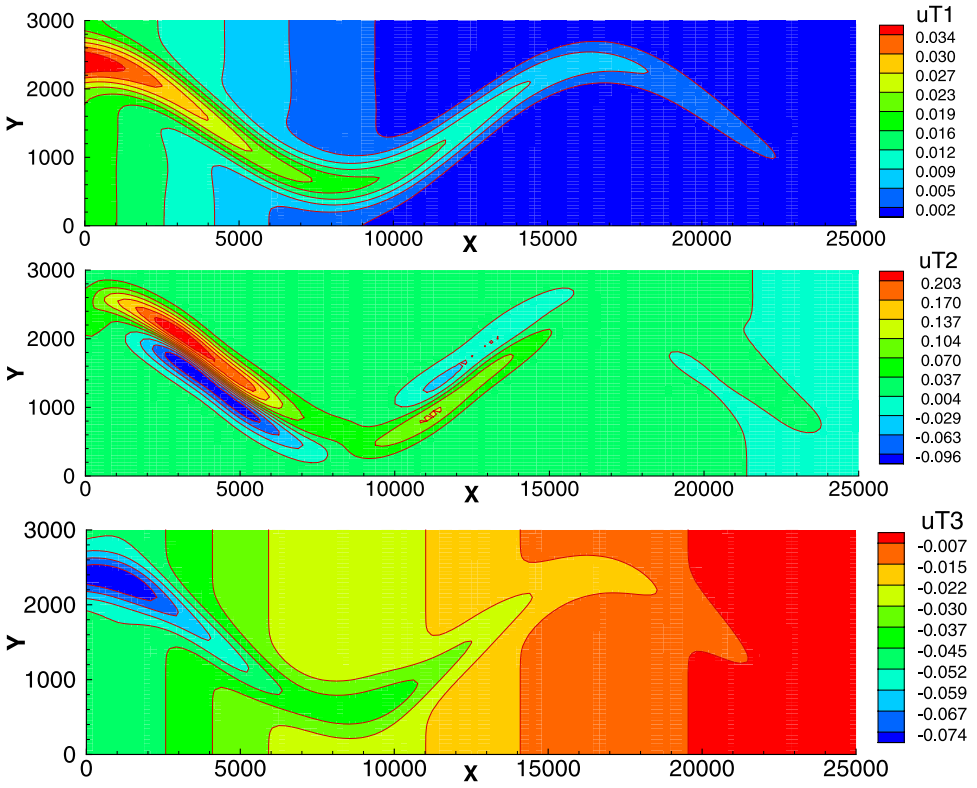

Figure 7. Residual velocity components contributed by the wave effect (u_{T1}), advection (u_{T2}), and pressure gradient (u_{T3}) for the bathymetry function defined in Figure 5b (L = 25 km).

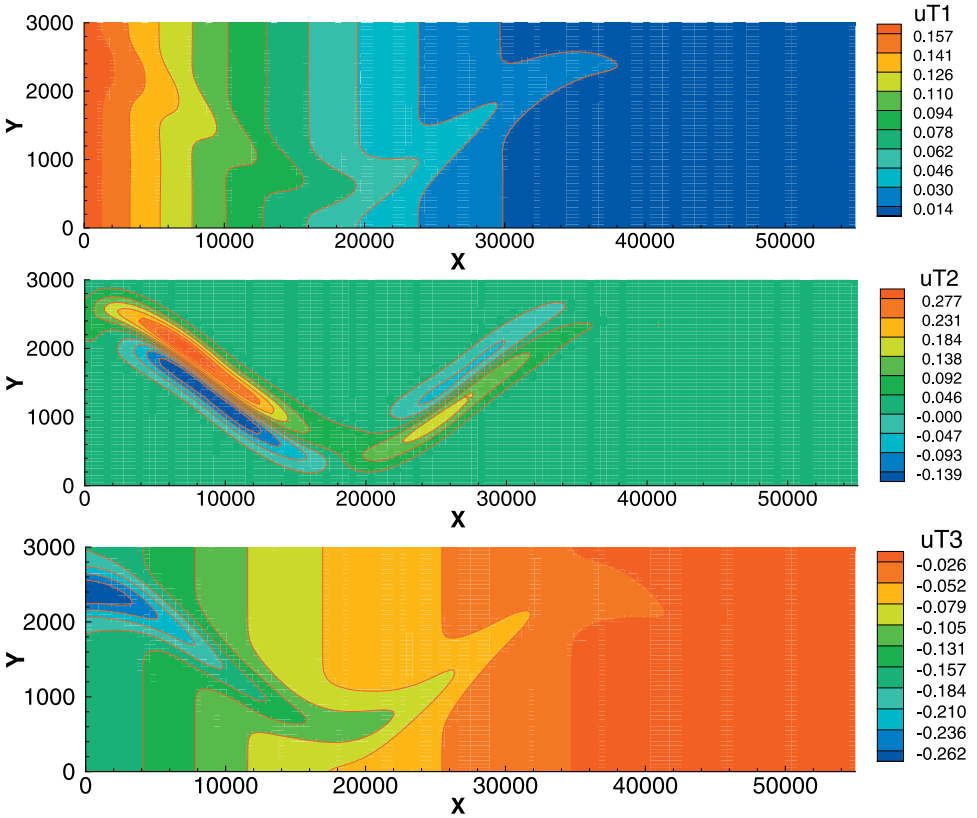

Figure 8. Residual velocity components contributed by the wave effect (u_{T1}), advection (u_{T2}), and pressure gradient (u_{T3}) for the bathymetry function defined in Figure 5c (L = 55 km).

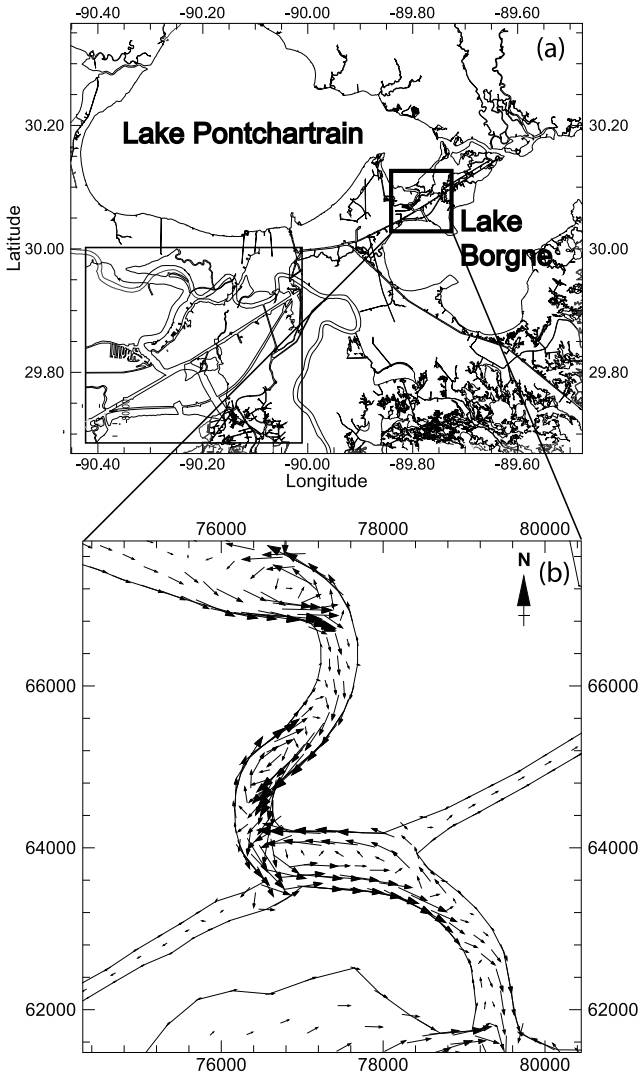

Figure 9. Study area for model application in southeast Louisiana–northern Gulf of Mexico: (a) Chef Menteur Pass and adjacent estuaries and (b) residual velocity vectors obtained from the FVCOM model results. The rectangular area shows an enlarged view of the model results in the channel.

average of the contributions from the first, second, and third terms are 7.3%, 45.0%, and 47.6%, respectively.

[41] For the first term, u_{T1}, it is found that about 76.4% of the points contribute to 0 to 10% of the net flow from u_{T1} (the majority of the points have small u_{T1} values). About 20.2% of the points have contributions between 10% and 30% and only 3.4% of these points have contributions greater than 30% of the net flow.

[42] For the second term, u_{T2}, it is found that 0.3% of these points have contributions to the total net flow below 10%; and 2.8% of the points have contributions between 10% and 30% of the net flow. About 64.5% of the points have contributions between 30% and 50% and 32.4% of the points have contributions greater than 50% of the net flow.

[43] For the third term, u_{T3}, it is found that there is no place within the model having contributions less than 10% of the net flow; while only 1.6% of the points have contributions between 10% and 30% of the net flow. About 60.9% of the points have contributions between 30% and 50% of the net flow; and 36.5% of the points have contributions between 50% and 70%. About only 1% of the points have contributions above 70% of the net flow.

[44] From these statistics, we may conclude that in general the first term has little contribution while the second and third terms have comparable contributions to the total net flow. This, however, is true with the understanding that at certain points, especially around the depth variations, the contributions from the first term can vary significantly and therefore the first term cannot be neglected in the momentum equation (the maximum contribution is 40% at certain points). *Li and O'Donnell* [2005] have discussed the effect of channel length on the residual circulation: a nondimensional length ratio δ, the ratio between the channel length and a quarter of the tidal wavelength, determines if the wave propagation effect (the first term u_{T1}) is important and if the mean flow regime falls into the long-channel ($\delta > 0.6$) or short-channel ($\delta < 0.6$) categories. In the present case, the channels are short and the first term of the residual velocity is generally small. This, however, does not imply that the frictional effect is negligible since the primary (or first-order) momentum balance is through the frictional force. The results for long channels are similar, although the first term becomes larger, as discussed earlier using the dimensional results. A similar discussion on the relative contributions is thus omitted here.

5. Numerical Model Results

[45] The analysis of the analytic model results have provided some insights to the major momentum balance in curved tidal channels and it has provided consistent results that can be used to explain the observed patterns. The model is however limited. The main limitation is that the model has to be rectangular, which is not a significant drawback as the bathymetry inside the rectangular area can be carved to have a meandering channel so that the effect of curvature can be captured nicely. The main problem is that the shoal depth cannot be too small to ensure the convergence of the model. Here, we present some numerical model results to further verify the findings from both the observations and the theoretical model. We use the unstructured grid finite volume coastal ocean model (FVCOM) developed by *Chen et al.* [2003]. The FVCOM is applied to the entire Lake Pontchartrain Estuary which has three major tidal passages connecting the coastal ocean with the low-salinity lake system: the Industrial Canal, the Rigolets, and the Chef Menteur Passes. The lake is about 40 km in the north-south direction and 60 km in the west-east direction (Figure 9a). For brevity, we will not show the details of the model grids (which are triangular in shape). We will only present the tidally averaged results of tidally induced flows.

[46] Chef Menteur Pass connects Lake Pontchartrain and Lake Borgne as shown in Figure 9a. It is a tidal pass with mean normal tidal flow of the order of 85,000 cubic feet per second ($\sim$2405 m^3/s). Normal tides in the area are diurnal with a typical range of 0.15 to 0.30 m. FVCOM was setup and applied in the Pontchartrain Basin. Boundary conditions for the model included diurnal tidal forcing, which was

applied at the open boundary, east of Lake Borgne (Figure 9a). Three dimensional velocities were simulated through the channel, and residual flow was computed. Figure 9b shows the structure of the depth-averaged residual flow in the channel after 45 d of simulation. The predicted residual transport velocity in the channel during the simulation period was 0.3 m/s with a standard deviation of 0.14 m/s. The vectors of the residual flow show a consistent eddy forming after each bent in the channel. The flow appears to be ebb dominant (northeastward directed), superimposed on the residual eddies. The numerical model results further verify the results from the analytic model. Note that the numerical model has meandering lateral boundaries, in contrast to the rectangular analytic model domain.

6. Summary

[47] This paper presents several full tidal cycle observations of residual flow field using vessel-based ADCPs in curved tidal channels. The main result from these observations is that the flow field across the channel tends to develop opposing currents, forming residual eddies near the curvature of the channel such that counterclockwise flows develop on the west side of the bend and clockwise flows develop on the east side of the bend (if the bend is toward the north). In the area of three channel conjunction of the Wilmington River, the flow is further modified by the complex geometry and a strong and persistent counterclockwise flow is developed.

[48] To further investigate the flow field in curved tidal channels, we have developed a nonlinear theoretical model. The model uses a double perturbation scheme and can allow arbitrary depth variations with one condition that the depth variation should be small to ensure that the perturbation expansions are convergent. We have used this model to conduct a series of experiments and verified the observed residual eddies.

[49] By analyzing the analytic model results, we conclude that the residual eddies are largely generated by the advection momentum. Although the pressure gradient and the nonlinear wave propagation may not be negligible, especially for long channels, it is the advection that generates the vorticity of the residual eddies. The conclusion is true for both short and long channels, a result different from that of straight channels [*Li and O'Donnell*, 2005]. The reason for the difference is that the curvature of the channel makes the advective momentum the most important term for both short and long channels.

[50] Finally, we have applied a numerical model (FVCOM) to the Lake Pontchartrain Estuary and results from a meandering tidal passage show the same type of residual eddies as observed and as in the analytic model. Future studies may include the examination of the change of importance of the curvature by varying the degree the river bends such that it may be made clear at what curvature would the effect of channel length be overshadowed by the curving of the channel. The effect of the exchange between the channel and wetland/saltmarsh can also be an interesting and practically useful study, either with models or observations.

[51] **Acknowledgments.** This work was supported by Georgia Sea Grant (RR746-007/7512067, R/HAB-12-PD, R/HAB-18-PD, RR746-011/7876867), Georgia DNR (RR 100-279-9262764), and National Science Foundation (OCE-0554674). Captains H. Carter and J. Fripp assisted in the field to collect the flow data. Two anonymous reviews helped the improvement of the manuscript. Editor Robert Weisberg also read the manuscript and provided critical comments that helped its improvement.

References

Blanton, J. O., G. Lin, and S. A. Elston (2002), Tidal current asymmetry in shallow estuaries and tidal creeks, *Cont. Shelf Res.*, *22*, 1731–1743.

Chant, R. J., and R. Wilson (1997), Secondary circulation in a highly stratified estuary, *J. Geophys. Res.*, *102*, 23,207–23,215.

Chen, C., H. Liu, and R. Beardsley (2003), An unstructured grid, finite-volume, three-dimensional, primitive equations ocean model: Application to coastal ocean and estuaries, *J. Atmos. Oceanic Technol.*, *20*(1), 159–186.

Dronkers, J. (1986), Tidal asymmetry and estuarine morphology, *Neth. J. Sea Res.*, *20*, 117–131.

Elston, S. A. (2005), Secondary circulation in a sinuous coastal plain estuary, Ph.D. dissertation, 321 pp., Ga. Inst. of Technol., Atlanta.

Elston, S. A., J. O. Blanton, and H. E. Seim (2000), Secondary circulation in curved and straight estuarine reaches, in *10th International Biennial Conference on Physics of Estuaries and Coastal Seas Proceedings*, *SRAMSOE Rep.366*, 172–175, Va. Inst. of Mar. Sci., Gloucester Point, Va.

Fang, G., and J. Yang (1985), A two-dimensional numerical model of the tidal motions in the Bohai Sea, *Chin. J. Oceanol. Limnol.*, *3*, 135–152.

Fares, Y. R. (1995), Boundary shear in curved channel with side overflow, *J. Hydraul. Eng.*, *121*, 2–14.

Fischer, H. B., E. J. List, R. C. Y. Koh, J. Imberger, and N. H. Brooks (1979), *J. Mixing in Inland and Coastal Waters*, 483 pp., Academic, San Diego, Calif.

Geyer, W. R. (1993), Three-dimensional tidal flow around a headland, *J. Geophys. Res.*, *98*, 955–966.

Hamrick, J. M. (1979), Salinity intrusion and gravitational circulation in partially stratified estuaries, Ph.D. dissertation, 451 pp., Univ. of Calif., Berkeley.

Hansen, D. V., and M. Rattray (1965), Gravitational circulation in straits and estuaries, *J. Mar. Res.*, *23*, 104–122.

Ianniello, J. P. (1977), Non-linear induced residual currents in tidally dominated estuaries, Ph.D. dissertation, 250 pp., Univ. of Conn., Storrs.

Ianniello, J. P. (1979), Tidally induced residual currents in estuaries of variable breadth and depth, *J. Phys. Oceanogr.*, *9*, 962–974.

Ikeda, S., and T. Nishimura (1986), Flow and bed profile in meandering sand-silt rivers, *J. Hydraul. Eng.*, *112*, 562–579.

Lacy, J. R., and S. G. Monismith (2001), Secondary currents in a curved, stratified, estuarine channel, *J. Geophys. Res.*, *106*, 31,283–31,302.

Li, C. (2002), Axial convergence fronts in a barotropic tidal inlet—Sand Shoal Inlet, VA, *Cont. Shelf Res.*, *22*, 2633–2653.

Li, C. (2006), Modeling of bathymetry locked residual eddies in well-mixed tidal channels with arbitrary depth variations, *J. Phys. Oceanogr.*, *36*, 1974–1993.

Li, C., and O'Donnell (1997), Tidally driven residual circulation in shallow estuaries with lateral depth variation, *J. Geophys. Res.*, *102*, 27,915–27,929.

Li, C., and O'Donnell (2005), The effect of channel length on the residual circulation in tidally dominated channels, *J. Phys. Oceanogr.*, *35*, 1826–1840.

Li, C., J. Blanton, and C. Chen (2004), Mapping of tide and tidal flow fields along a tidal channel with vessel-based observations, *J. Geophys. Res.*, *109*, C04002, doi:10.1029/2003JC001992.

Li, C., S. Armstrong, and D. Williams (2006), Residual eddies in a tidal channel, *Estuaries Coasts*, *29*, 147–158.

Li, C., A. Valle-Levinson, L. P. Atkinson, and T. C. Royer (2000), Inference of tidal elevation in shallow water using a vessel-towed acoustic Doppler current profiler, *J. Geophys. Res.*, *105*, 26,225–26,236.

Maddock, L., and R. D. Pingree (1978), Numerical simulation of the Portland tidal eddies, *Estuarine Coastal Mar. Sci.*, *6*, 353–363.

Parker, B. B. (1984), Frictional effects on the tidal dynamics of shallow estuary, Ph.D. dissertation, 291 pp., Johns Hopkins Univ., Baltimore, Md.

Pietrafesa, L. J., J. O. Blancton, J. D. Wang, V. Kourafalou, T. N. Lee, and K. A. Bush (1985), The tidal regime in the South Atlantic Bight, in *Oceanography of the Southeastern Continental Shelf*, *U.S., Coastal Estuarine Stud.*, vol. 2, edited by L. P. Atkinson, D. W. Menzel, and K. A. Bush, pp. 63–76, AGU, Washington, D. C.

Pingree, R. D. (1978), The formation of the shambles and other banks by tidal stirring of the seas, *J. Mar. Biol. Assoc. U. K.*, *58*, 211–226.

Pingree, R. D., and L. Maddock (1977a), Tidal residuals in the English Channel, *J. Mar. Biol. Assoc. U. K.*, *57*, 339–354.
Pingree, R. D., and L. Maddock (1977b), Tidal eddies and coastal discharge, *J. Mar. Biol. Assoc. U. K.*, *57*, 869–875.
Pingree, R. D., and L. Maddock (1979), The tidal physics of headland flows and offshore tidal bank formation, *Mar. Geol.*, *32*, 269–289.
Proudman, J. (1953), *Dynamical Oceanography*, 409 pp., Methuen, New York.
Seim, H., and M. C. Gregg (1997), The importance of aspiration and channel curvature in producing strong vertical mixing over a sill, *J. Geophys. Res.*, *102*, 3451–3472.
Signell, R. P., and W. R. Geyer (1991), Transient eddy formation around headlands, *J. Geophys. Res.*, *96*, 2561–2575.
Simpson, J. H., J. Brown, J. Matthews, and G. Allen (1990), Tidal straining, density currents, and stirring in the control of estuarine stratification, *Estuaries*, *13*, 125–132.
Valle-Levinson, A., C. Reyes, and R. Sanay (2003), Effects of bathymetry, friction, and rotation on estuary-ocean exchange, *J. Phys. Oceanogr.*, *33*, 2375–2393.
Wolanski, E., T. Asaeda, A. Tanaka, and E. Deleersnijder (1996), Three-dimensional island wakes in the field, laboratory experiments and numerical models, *Cont. Shelf Res.*, *16*, 1437–1452.
Wong, K.-C. (1994), On the nature of transverse variability in a coastal plain estuary, *J. Geophys. Res.*, *99*, 14,209–14,222.
Ye, J., and J. A. McCorquodale (1998), Simulation of curved open channel flows by 3D hydrodynamic model, *J. Hydraul. Eng.*, *124*, 687–698.

C. Chen, School for Marine Science and Technology, University of Massachusetts Dartmouth, 706 South Rodney French Blvd., New Bedford, MA 20744, USA.
I. Y. Georgiou, Department of Earth and Environmental Sciences, University of New Orleans, 2000 Lakefront, New Orleans, LA 70148, USA.
D. Guadagnoli, Coastal Resources Division, Department of Natural Resources, One Conservation Way, Brunswick, GA 31520, USA.
C. Li, Coastal Studies Institute, Department of Oceanography and Coastal Sciences, Louisiana State University, Baton Rouge, LA 70803, USA.